A&A manuscript no.
(will be inserted by hand later)

Your thesaurus codes are:
01(03.20.4; 08.09.2 Eta Carinae; 08.03.4; 08.09.1)

ASTRONOMY
AND
ASTROPHYSICS
19.12.1995

Speckle-masking imaging polarimetry of η Carinae: evidence for an equatorial disk

Heino Falcke[1,2], Kris Davidson[3], Karl-Heinz Hofmann[1], Gerd Weigelt[1]

[1] Max-Planck Institut für Radioastronomie, Auf dem Hügel 69, D-53121 Bonn, Germany (weigelt@mpifr-bonn.mpg.de)
[2] Department of Astronomy, University of Maryland, College Park, MD 20742-2421, USA (hfalcke@astro.umd.edu)
[3] Astronomy Department, University of Minnesota, 116 Church St., Minneapolis, MN 55455, USA

Accepted for publication in A&A Letters (Dec. 19, 1995) – in press

Abstract. With our new speckle imaging polarimeter we have obtained the first polarimetric images with sub-arcsecond resolution of the Luminous Blue Variable η Carinae in the Hα line. The polarization patterns at the 3" scale match well earlier conventional imaging photometry and can be interpreted as Mie scattering. In crosscorrelation-centered images we detected in polarized light a bar in the NE part of the equatorial plane of η Carinae. High-resolution 0.11" polarimetric speckle reconstructions reveal a compact structure elongated in the same direction which is consistent, in degree and position angle of the polarisation, with the presence of a circumstellar, equatorial disk. The degree of polarization of the previously discovered speckle objects and the Hα arm is relatively low ($\sim 10\%$) and thus may indicate a position within the equatorial plane. We also discovered a highly polarized ($20\% - 40\%$) bipolar structure along the major axis of the Homunculus nebula which can be traced down to the sub-arcsecond scale. This is probably the inner part of a bipolar outflow into the Homunculus.

Key words: techniques: polarimetric – stars: individual: Eta Carinae – circumstellar matter – stars: imaging

1. Introduction

Because of its extraordinary luminosity of $\sim 10^{6.6} L_{\odot}$ the Luminous Blue Variable η Carinae is one of the most interesting objects for the understanding of the late evolutionary stages of massive stars (see Humphreys and Davidson 1994, and references therein). It is embedded in the Homunculus, a bi-polar nebula oriented at PA 132°, which is reflecting light from the central object. η Carinae was also one of the earliest complex structures that was successfully studied at sub-arcsec resolution by speckle methods. Weigelt & Ebersberger (1986) and Hofmann & Weigelt (1988) found 3 objects close to the central star (0.1-0.2" separation); first HST UV observations of the speckle objects were reported by Weigelt et al. (1995). They appear very compact in far-red light; but since they are moving outward (Weigelt et al. 1995 & 1996) and have forbidden lines in their spectra (Davidson et al. 1995), they must be ejected clouds rather than companion stars. In Hα the sub-arcsecond structure of η Carinae is even more complex, showing an arm-shaped feature in the north (Weigelt et al. 1996).

Polarization observations have shown that η Carinae is intrinsically polarized (Visvanathan 1967, Marraco et al. 1993). Warren-Smith et al. (1979) showed that the total polarization of the Homunculus is always perpendicular to the direction to the central object as expected for Mie scattering by dust grains. In the outer regions the degree of polarization reaches up to 40% while in the inner regions it is well below 10% (see also Meaburn et al. 1993). Dust is expected to form at roughly the same distance from the star as the speckle objects.

To extend those studies we have built a polarimeter for our speckle camera and are now for the first time able to obtain high-resolution polarimetric information at optical wavelengths with ground-based telescopes. Here we report on results we obtained during a first test-run of our speckle imaging polarimeter where we observed η Carinae with an Hα filter.

2. Observations

2.1. The polarimeter

Our new polarimeter consists mainly of a rotatable, achromatic $\lambda/2$-retardation mica plate in front of a fixed polarization filter. If rotated by an angle α the $\lambda/2$ plate rotates the polarization vector of the incident light by 2α. The usable wavelength range is 450-800 nm with an error for the retardation of 2% of $\lambda/2$ over the whole wavelength range and a transmission of $\sim 70\%$. The polarization filter has a transmission of $\sim 33\%$ and a polarization degree of $> 99.99\%$ over a wavelength range of 450-750nm. The $\lambda/2$-plate is mounted on a remote-controlled rotator with a step motor of 1/500 Degree resolution. Filter, rotator and $\lambda/2$-plate were installed on a single mount that was inserted into the optical axis in front of the telescope focus of our camera. The use of a fixed polarization filter basically eliminates the effects of depolarization in the camera, as the polarization vector of the light entering the camera has always the same orientation. Circular polarization can not be measured.

2.2. Observing strategy

η Carinae was observed with the ESO 2.2 m telescope in Chile on March 12, 1995 between ST 12:20 and ST 12:50 with an improved version of our MPIfR speckle camera (Baier & Weigelt 1983) using a 30 nm wide Hα filter and 20 fold magnification giving us a field of view of ~ 6 arcsec. In total we took 4800 images of 50 ms exposure time at a frame rate of 4 images/sec including flatfield and dark images. The observation was split into 16 sections of 300 images each. After each section we rotated the $\lambda/2$-plate by 22.5° corresponding to a rotation of 45° of the incident polarization vector. We finally obtained four independent measurements of the polarized intensity for each of the four possible orientations of the polarization vector (0°, 45°, 90°, and 135°). This has the benefit that we have a full rotation of the $\lambda/2$-plate and two rotations of the polarization vector with respect to the polarization filter which helps to detect and reduce the effects of any rotational asymmetries in the polarimeter. A second advantage of taking interleaved images is that the images for each 45° rotation of the polarization vector – if added together – are taken quasi-simultaneously thus a slow monotonic change in the seeing conditions affects all images in a similar way. This is especially important for the reconstruction of speckle images. Finally, we want to note that the use of a speckle camera does have another intrinsic advantage over conventional imaging polarimetry: by evaluating the total intensities of all images we can monitor the short-time variability of the atmospheric transmission.

After the observation we measured a flatfield to determine the photonbias (Pehlemann et al. 1992) and a single star (SAO251486) to obtain the speckle transfer function. The same observations as for η Carinae were performed thereafter with a nearby cluster member (HDE 303308) for comparsion.

3. Data reduction

3.1. Total polarization

Prior to the data reduction we combined the four small data sets for each polarization angle into a large data set containing 1200 images each. During the speckle-masking reconstruction of the images the information of the total intensity is lost and therefore one has to re-scale the intensity according to the intensities of the co-added long-exposure images. One way to achieve this would be to simply co-add all images and determine the degree of polarization from the four long-exposure images. However, using this method, we would loose the valuable informaton of the short-term variability of our data. Therefore, we extracted the (image-intensifier dark subtracted) integrated intensities of each image and plotted them in the order they had been obtained originally. Although the seeing was relatively stable and we had perfect weather conditions, we found small variations of the integrated short-exposure image intensities of η Carinae of the order of a few per cent, clearly exceeding the instrumental noise in amplitude. The run of intensities can be described by a constant upper envelope plus occasional, erratic dips. We interpret this as short-term reduction of the atmospheric transmission from the optimal value; an uneven distribution of those dips among the different polarization angles would clearly affect any polarization results based on the usual average (as in long exposures). A simple way to eliminate the influence of those dips is to take the median value of an upper constant envelope of the intensities, e.g. the brightest N of all images. Indeed we found that by varying N and calculating the deviation of the polarized intensity from the expected Sinus shape the error has a well defined minimum around $N = 16\%$, yielding a degree of polarization of $P = 4.06\%$ and a position angle (PA) for the E-vector of $\theta_{\rm P} = 73.5°$ for our field of view. Nevertheless, the results differed only by $\pm 0.025\%$ in P and $\pm 0.5°$ in $\theta_{\rm P}$ over a range of $N = 10\% - 60\%$ (which would include the 'normal' median).[1]

The situation for the cluster star HDE 303308 was slightly different as it is substantially fainter than η Carinae and the intensity variations are mainly dominated by photon and instrumental noise. Hence, we took the usual median intensities for the four polarization angles at $N = 50\%$ – where the minimum error was found – yielding $P = 2.76\%$ and $\theta_{\rm P} = 102\%$. Here, the systematic variations by changing N are $\pm 0.3\%$ and $\pm 5°$ respectively. We noticed a 100 times fainter companion $3.4''$ away from HDE 303308 at PA 231°.

3.2. Image reconstruction and polarization maps

From the four combined data sets we reconstructed four images using the basic speckle-masking technique as described in Weigelt (1977), Lohmann et al. (1983), and Hofmann & Weigelt (1986). To ensure that the reconstructions of all images were done in an identical manner, we used the automatized speckle processing package (ASP) recently developed at the MPIfR (Falcke et al. 1996).

The basic scheme of the automated speckle data reduction process consists of the following steps: image intensifier dark current and flatfield corrections, detection of ion contamination, seeing selection, calculation of crosscorrelation-centered images, photon-bias compensation, bispectrum calculation, and image reconstruction. Thus we obtained images at different resolutions up to the diffraction limit. Our diffraction-limited Hα total intensity image confirms the detections by Weigelt et al. (1996) and especially shows the northern $H\alpha$-arm and its blobs and even the weak features to the SE and NE of the nucleus.

To obtain our polarization map, we first determined the position of the central peak in each image by fitting a two-dimensional gaussian and shifted each image onto a common center. We then normalized the total intensity of the reconstructed images according to the values found in Section 3.1. From the four shifted and normalized images corresponding to the four polarization angles we determined the Stokes parameters for each pixel and the standard deviation from a sinusoidal distribution. In the polarization maps we left out all vectors having errors $> 30\%$ although mostly the errors are $< 10\%$. For the vector maps we usually also combined four pixels for one vector. Most affected by errors are the polarization angles in the fainter parts of the reconstructed image and we have not made any attempt to correct the interstellar polarization in the Hα line towards η Carinae.

4. Results

In Fig. 1a we show the contours of the crosscorrelation-centered 6×6 arcsec total intensity image of η Carinae overlayed with the vectormap of the polarization. The tangential pattern of the polarization vectors is in good agreement with the results by Warren-Smith et al. (1979); this is best seen in the NW spur where the polarization reaches values of 20-40%. The bipolar nature of the Homunculus becomes apparent in the polarized

[1] For this extended object, however, the total polarization vector of our small square aperture can not easily be compared with usual large round apertures.

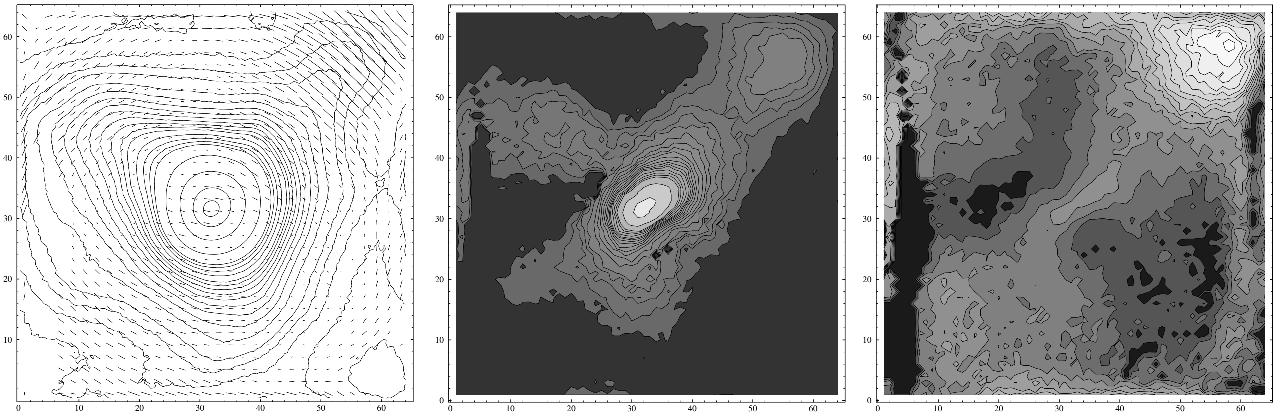

Fig. 1. a) Crosscorrelation-centered 6×6 arcsec image of η Carinae and its polarization – north is up and east to the left. The short lines indicate the orientation of the E-vector and the length is proportional to the degree of polarization. b) The total polarized flux of the left image. c) The per-cent polarization of the left image. The images were zoomed from our 512^2 format down to a 64^2 format. The distortions at the edges of the images are consequences of the centering procedure.

light (Fig. 1b&c) and there is also a bar along the minor axis (PA 42°) towards the NE, which is already present in the total intensity map but becomes a marked feature in the polarized intensity map (Fig. 1b). There may also be a very weak SW counterpart which is, however, not well visible in the contour plots. Figure 1c shows that the degree of polarization is asymmetric with respect to the center and is lower towards the SE and higher in the NW. The degree of polarization seems to be reduced in a strip along the minor axis and the central object appears elongated. Such a pattern can be found if the central star itself is polarized (Elsässer & Staude 1978; Gledhill 1990).

In Fig. 2a we show the contour map of the Hα speckle-masking reconstruction of the inner arcsecond of the Homunculus and its polarization. To increase the SNR of the polarization map we have not reconstructed the image up to the diffraction limit but with a lower resolution of 0.11 arcsec. At the central peak the polarization is $P = 9.1\%$ and $\theta_{\rm P} \simeq 80°$. It is remarkable that the largest part of the Hα arm and the four speckle objects A-D are in a region of relatively low polarization around 10%. The PA of the polarization vectors of the three speckle objects B-D are similar to those of the central star and almost perpendicular to the radial axis towards the center. The polarization increases strongly towards the NW where it still is perpendicular to the radial axis and $P = 20 - 40\%$. This feature connects well into the NW spur seen already in Fig.1a.

It is also noteworthy that the total intensity of η Carinae in the high-resolution image is sharply reduced below the minor (NE-SW) axis. In the polarized intensity map (Fig. 1b) we do see several co-linear blobs along the same axis which are symmetric around the center. We note that this linear feature also connects the NE end of the northern arm and the central star. In a larger field of view it also continues smoothly into the bar noted already in Fig.1 while there is no such strong feature in the SW on the larger scale.

5. Summary and Discussion

Hα observations of the LBV η Carinae during a first test run of our polarimeter have demonstrated the feasibility of optical speckle imaging polarimetry. Degree and PA of the polarization of the reference star HDE 303308 agree within the errors with the literature values (Visvanathan 1976; Marraco et al. 1993), the outer polarization pattern of our η Carinae image itself match well the inner structure found by Warren-Smith et al. (1979) and the high-resolution reconstruction of η Carinae confirms the structures detected by Weigelt et al. (1996). Several large-scale features continue down to the small scales.

Along the minor axis of the Homunculus we have detected a bar to the NE of η Carinae in the polarized light and we find a linear symmetric structure in the inner arcsecond which is oriented in the same direction. This, together with the sharp intensity drop from the NW to the SE in the high-resolution image and the constriction of the central contours on the larger scale may be indicative of the presence of a dusty equatorial disk around η Carinae with its rotation axis along the major axis of the Homunculus. The NE bar and the central arcsecond bar could then be interpreted as scattered light from the surface of the disk. This may explain the PA and the high degree of the polarization in the NE and SW blobs in Fig. 2b. The absence of a SW counterpart to the NE bar on the large scale (while present at the sub-arcsecond scale) might be explained by a warped or distorted geometry. The up-turn of the NE end of the Hα arm seen in this paper and by Weigelt et al. (1996) could be indicative of a physical connection between the arm and the putative disk.

The usual explanation of the brightness contrast between the parts above and below the minor axis would be obscuration by the disk. The SE side of the homunculus polar axis points obliquely *towards* us, as seen in velocity data (Thackeray 1961, Meaburn et al. 1987) and in modern high-resolution images (Duschl et al. 1995, Humphreys & Davidson 1994). Material oriented along the polar axis would therefore be more visible on the SE (nearer) side and obscured on the NW side, exactly the opposite to what is observed near the star. Hence we conclude that most of the small-scale structure discussed above is essentially equatorial rather than polar: we are seeing the most visible inner NW parts of the equatorial ejecta-disk pointing towards us.

This picture is consistent with the low polarization of the speckle objects and the H-alpha arm ($\lesssim 10\%$), since Mie scattering produces lower polarization at relatively small scattering angles. We also point out that the polarization properties of

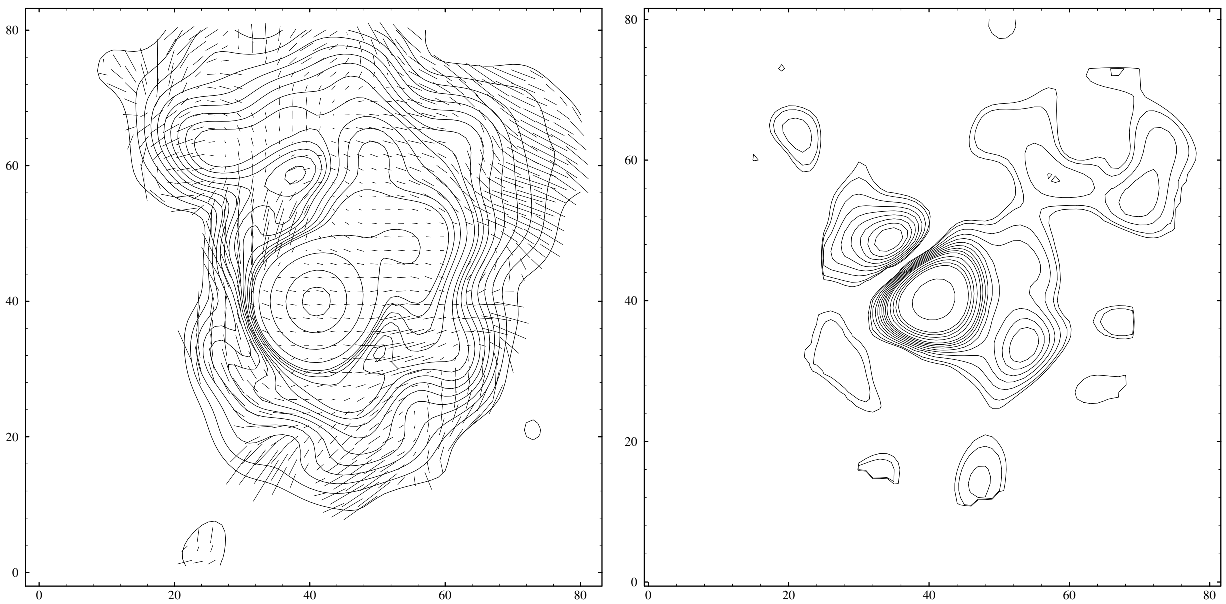

Fig. 2. a) Contour map of the Hα speckle-masking reconstruction and E-vector map of η Carinae for a 0.94×0.94 arcsec field (north is up, east to the left). The resolution is artificially degraded to 60% of the diffraction limit corresponding to 0.11 arcsec for the benefit of a higher SNR. The short lines indicate the orientation of the E-vector and the length is proportional to the degree of polarization. b) The total polarized flux of the left image. The hole at (65,65) in the NW structure corresponds to a high-error pixel which was left out.

the central star and the speckle objects B-D are basically indistinguishable even though the latter are clearly scattered light from the nucleus (Davidson et al. 1995), hence in the nucleus we may see in the polarized light a dusty envelope (or disk) rather than the naked star alone, and the speckle objects B-D as well as the Hα arm might well be part of the disk and its radial streamers (see Duschl et al. 1995). That the central star is most likely obscured was already evident from earlier observations where it was shown that the bright nucleus is extended and much too faint with respect to the surrounding speckle objects B-D (Weigelt et al. 1995).

Some of the H-alpha light observed in the speckle objects and the H-alpha arm may be emitted there, rather than scattered – unlike the case for larger size scales in the homunculus. This would of course be consistent with low polarizations. Further observations in continuum light may show larger amounts of polarization, since most *continuum* light in the blobs is expected to be scattered from the central star. In addition to the speckle objects and the Hα arm we also find at the subarcsecond scale something which might be the continuation of the NW spur seen in Figure 1. It appears in the polarized intensity image (Fig. 2b) but is barely visible in normal intensity (Fig. 2a). The polarization of this feature is very high (up to 40%), indicating large scattering angles and suggesting that this feature is part of the low-density, highly polarized NW part of the Homunculus nebula rather than a part of the disk.

We conclude that our findings support the model of an equatorial disk surrounding η Carinae. The presence of such a disk can be very important for the angular momentum loss in the late phases of massive stars – if it is an excretion disk, as indicated by the radial streamers (often referred to as jets). Still, we have to await further observations as from this test run we had only a limited number of images available for our reconstruction.

Acknowledgements. HF was supported by a Max-Planck Stipend. We thank P.L. Biermann for stimulating comments and R. Österreicher and C. Möllenhoff for helpful discussions on imaging polarimetry.

References

Baier G., Weigelt G. 1983, A&A 121, 137

Davidson K., Dufour R.J., Walborn N.R., Gull T.R. 1986, ApJ 305, 867

Davidson K., Ebbets D., Weigelt G., Humphreys R.M., Hajian A.R., Walborn N.R., Rosa M. 1995, AJ 109, 1784

Duschl W.J., Hofmann K.-H., Rigaut F., Weigelt G. 1995, RevMexAA (Serie de Conferencia) 2, 17

Elsässer H., Staude H.J. 1978, A&A 70, L3

Falcke H. et al. 1996, in prep.

Gledhill T.M. 1990, MN 252, 138

Hofmann K.-H., Weigelt G. 1986, A&A 167, L15

Hofmann K.-H., Weigelt G. 1988, A&A 203, L21

Humphreys R.M., Davidson K. 1994, PASP 106, 1025

Lohmann A., Weigelt G., Wirnitzer B. 1983, Apl.Opt. 22, 4028

Meaburn J., Walsh J., Wolstencroft R. 1993, A&A 268,283

Meaburn J., Wolstencroft R., Walsh J. 1987, A&A 181, 333

Marraco H.G., Vega E.I., Vrba F.J. 1993, AJ 105, 258

Pehleman E., Hofmann K.-H., Weigelt G. 1992, A&A 256, 701

Thackeray, A.D. 1961, Observatory 81, 99

Visvanathan N. 1967, MNRAS 135, 275

Warren-Smith R.F., Scarrott S.M., Murdin P., Bingham R.G. 1979, MNRAS 187, 761

Weigelt G. 1977, Opt. Commun. 21, 55

Weigelt G., Ebersberger J. 1986, A&A 163, L5

Weigelt G., Davidson K., Hofmann K.-H. 1996, A&A subm.

Weigelt G., Albrect R., Barbieri C. et al. 1995, RevMexAA (Serie de Conferencia) 2, 11